Scintillation characteristics of annular beam array in underwater optical links

Erdoğdu, Ekin; Gökçe, Muhsin Caner; Baykal, Yahya

DOI
10.1088/2040-8986/ae059c

Publication date
2025

Document Version
Final published version

Published in
Journal of Optics

Scintillation characteristics of annular beam array in underwater optical links

OPEN ACCESS
IOP Publishing
Journal of Optics
J. Opt. **27** (2025) 095603 (9pp)
https://doi.org/10.1088/2040-8986/ae059c

Scintillation characteristics of annular beam array in underwater optical links

Ekin Erdoğdu[1], **Muhsin Caner Gökçe**[2,3,*] **and Yahya Baykal**[1]

[1] Department of Electrical-Electronics Engineering, Çankaya University, Yukarıyurtçu mah. Mimar Sinan cad. No: 4, Etimesgut, Ankara 06815, Türkiye
[2] Department of Geoscience and Remote Sensing, Delft University of Technology, 2628 CD Delft, The Netherlands
[3] Department of Electrical-Electronics Engineering, TED University, Ankara 06420, Türkiye

E-mail: m.c.gokce@tudelft.nl, ekinerdogduu@gmail.com and y.baykal@cankaya.edu.tr

Received 17 June 2025, revised 22 August 2025
Accepted for publication 10 September 2025
Published 19 September 2025

Abstract

Underwater optical wireless communication systems offer a promising alternative to traditional acoustic methods for achieving high data rate transmission. However, the propagation of optical waves in underwater environments is severely impacted by oceanic turbulence, leading to intensity fluctuations and consequent performance degradation. In this work, we employ a laser beam array to model transmit spatial diversity for suppressing these fluctuations. The model uses annular-shaped lasers at the transmitter as a representation of beam shaping for turbulence mitigation, with a point detector assumed at the receiver. Through the use of the Huygens–Fresnel principle, we derive two key optical parameters: the average received intensity and the average of the intensity squared. We subsequently determine the scintillation index for this model. Our findings demonstrate reductions in scintillation under varying system parameters. For instance, increasing the number of beams in the array, the ring radius, and the secondary field amplitude of the annular beam leads to a lower scintillation index.

Keywords: annular beam array, oceanic turbulence, optical beam shaping, optical wave propagation, scintillation index

1. Introduction

Underwater optical wireless communication (UOWC) is an innovative technology offering high-bandwidth, high-data-rate, and secure communication between underwater terminals, overcoming the constraints of traditional acoustic methods. With these advantages, future technologies such as machine-to-machine communication, high-volume remote computing, and the internet of things are expected to incorporate UOWC systems, capable of supporting thousands of mobile end-users and exceptionally high data rates. This expected advancement, however, will bring forth substantial challenges and necessitate the development of innovative strategies to mitigate the degrading effects of the underwater medium [1, 2].

There are three main degrading effects that hinder light propagation underwater: absorption, scattering, and oceanic turbulence. Absorption and scattering are primarily wavelength-dependent and can be mitigated by using the transparent wavelength ranges in seawater, such as the blue and green portions of the electromagnetic spectrum [3]. The studies have provided detailed insights into how visible light beams are affected by absorption and scattering in pure water [4]. In detail, chlorophyll concentration is the primary factor responsible for attenuation losses in the underwater environment [5]. The absorption and scattering of light by suspended particles and dissolved substances in underwater reduces the signal strength, resulting

* Author to whom any correspondence should be addressed.

in weaker signals and shorter transmission distances. On the other hand, oceanic turbulence occurs due to temperature and salinity fluctuations, which cause intensity fluctuations in the propagating beam, as well as beam spreading and wandering.

There are techniques to mitigate the effects of oceanic turbulence, such as spatial diversity, beam shaping, aperture averaging, the use of intelligent reflecting surfaces, and partially coherent beams. Among these, this study investigates transmit spatial diversity, achieved by employing multiple spatially separated laser beams at the transmitter, along with the laser beam shaping method. The spatial diversity at the transmitter, known as multiple-input single-output (MISO), plays an important role in reducing the scintillation and overcoming the limitations of transmitted optical power [6]. Additionally, transmit diversity helps to minimize pointing errors [6]. Beam shaping is also recognized as a turbulence mitigation tool, achieved by modifying the light beam using optical lenses or spatial light modulators. In practice, UOWC systems typically rely on commercial laser beams with Gaussian-shaped optical field distributions. Transforming the laser beam into non-Gaussian shapes, such as annular, vortex, or flat-topped profiles, can enhance its resistance to oceanic turbulence [7]. Moreover, aperture averaging is another technique employed in UOWC systems. This approach involves enlarging the receiver aperture to smooth the distorted wavefront and improve the received signal-to-noise ratio (SNR) [8]. Additionally, the use of intelligent reflecting surfaces in UOWC systems is widely adopted. These surfaces consist of programmable elements that can reflect incident signals in a controlled manner to enhance communication performance. For example, when light strikes these surfaces, its amplitude can be enhanced, and its phase can be adjusted, which enhances signal quality and increases the communication range underwater [9]. Lastly, the partial coherent beam is formed by deforming the beam's coherence with a diffuser, which helps reduce scintillation at the receiver. However, the increased beam spreading may cause a reduction in the received intensity [10, 11]. All of the aforementioned methods offer certain advantages for reducing scintillation and improving the received power; however, in some underwater scenarios, their implementation in a UOWC system is challenging due to system complexity, the dynamic nature of the aquatic environment, and high cost. In this paper, we focus on combining transmit spatial diversity and beam shaping, as both are widely recognized techniques for turbulence mitigation and can be conveniently modeled analytically using the annular beam array source formula. Notably, employing these two methods together results in a lower scintillation compared to using either method alone for a specific set of system parameters.

The literature extensively examines the performance of transmit diversity techniques in OWC systems operating in underwater environments. In [12], a closed-form expression for the ergodic capacity of MISO UOWC systems is derived, and the effects of spatial repetition coding and transmit laser selection on MISO UOWC performance are discussed. In [13], the error probability of a spatial diversity UOWC system over a log-normal turbulence channel is derived, considering the effects of absorption, scattering, and oceanic turbulence, and the theoretical findings are validated through numerical simulations. In [14], the scintillation index and SNR of parallel and tilted MISO UOWC systems employing aperture averaging are analyzed by using wave optics simulation method. The findings indicate that increasing the number of laser beams reduces scintillation and improves the SNR. The study also emphasizes the advantages of tilted beams compared to parallel beams. In [15], the effect of convergent beam array on reducing the scintillation index and beam spreading between misaligned transceivers has been reported by multistep wave optics simulation. The authors in [16] reported that, by adjusting the pointing directions of each individual beam using reflectors, they aimed to reduce path loss and scintillation, as well as to minimize the impact of pointing errors. The study provides a detailed analysis of pointing errors, path loss, scintillation index, and bit-error rate (BER). In [17], a laser array beam is used at the transmitter, and the scintillation index and BER at the detector are reported. The laser array beam is also utilized in free-space optical links to examine transmit diversity [18, 19]. In [20], the BER performance of a single-input multiple-output UOWC system employing on-off keying modulation, optical pre-amplification, and equal gain combining are reported under the effects of a log-normal turbulence channel. Spatial diversity can be employed at both the transmitter and receiver, forming a multiple-input multiple output (MIMO) system. In [21], an analytical expression for the outage performance of MIMO UOWC systems is presented using the Meijer-G function. The study examines the effects of underwater turbulence, pointing errors, attenuation, and angle-of-arrival fluctuations on the outage performance. Furthermore, Jamali *et al* [22] analyzed the exact and upper bound BER performance of a MIMO UOWC system, considering the effects of absorption, scattering, and underwater oceanic turbulence. Additionally, Jamali *et al* analyze underwater visible light communication performance, utilizing spatial diversity and detection techniques to reduce fading and intersymbol interference [23]. Finally, in [24], Jiang *et al* study DC-biased optical orthogonal frequency division multiplexing visible light communication with spatial diversity in turbulence. They derive and validate bit error rate BER expressions and show that spatial diversity helps reduce fading and improves system design.

In this paper, we analyze a MISO UOWC system that utilizes an annular laser beam array at the transmitter and a point detector at the receiver. The propagation of optical waves from the annular beam array, influenced by oceanic turbulence, is examined using the Huygens–Fresnel principle. To compute the scintillation index at the detector, we first derive a closed-form expression for the average intensity, followed by the average of the squared intensity at the receiver. The scintillation index is a crucial performance metric for UOWC systems, as it reflects fluctuations in the received signal intensity,

leading to an increase in the BER. This study explores how various system parameters, such as the number of annular laser beams, ring radius, optical field amplitude, oceanic turbulence characteristics, and laser wavelength, affect the scintillation index.

2. Formulation

2.1. System model

We investigate an underwater optical communication system that incorporates multiple annular laser sources at the transmitter and a point detector situated horizontally at a distance of L meters from the transmitter. Additionally, as the optical beam propagates through oceanic turbulence, wave distortions occur, leading to scintillation. A visual representation of our proposed model is shown in figure 1

The transmitter in our proposed system model is mathematically represented by the optical field expression of an annular beam array, which is

$$u_N(\mathbf{s}) = \sum_{n=1}^{N} A_1 \exp\left\{-\frac{1}{2\alpha_{s1}^2}\left[s_x^2+s_y^2-2r_0(s_x\cos\theta_n + s_y\sin\theta_n - 0.5r_0)\right]\right\} - A_2\exp\left\{-\frac{1}{2\alpha_{s2}^2}\left[s_x^2+s_y^2-2r_0(s_x\cos\theta_n + s_y\sin\theta_n - 0.5r_0)\right]\right\}. \quad (1)$$

Here, the array consists of N annular beams, each with a primary (outer) source size α_{s1} and a secondary (inner) source size α_{s2}. A_1 and A_2 represent the field amplitudes of outer and inner beams, respectively, in volts per meter ($\mathrm{V\,m^{-1}}$), $s=(s_x,s_y)$ is the transmitter plane spatial coordinates. Furthermore, the annular beams are positioned on a ring with radius r_0, and each beam's location is determined by the angle $\theta_n = 2\pi(n-1)/N$. We can reformulate (1) to derive a single expression as follows

$$u_{Ns}(\mathbf{s}) = \sum_{n=1}^{N}\sum_{n1=1}^{2} A_{n1}\exp\left\{-\frac{1}{2\alpha_{sn1}^2}\left[s_x^2+s_y^2-2r_0(s_x\cos\theta_n + s_y\sin\theta_n - 0.5r_0)\right]\right\}. \quad (2)$$

We utilize (2) to simplify the evaluation of the average of the intensity squared provided in (19).

2.2. Equivalent structure constant for oceanic turbulence

In this section, we represent the equivalent structure constant in terms of oceanic turbulence parameters by applying the method outlined in [25]. Baykal suggested that by equating the spherical wave scintillation index solutions in the boundary layers of oceanic and atmospheric turbulence, the equivalent structure constant can be derived using parameters from

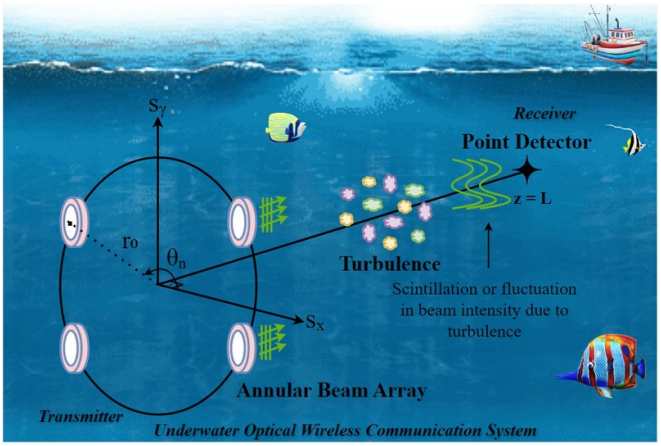

Figure 1. System model for underwater optical wireless communication.

underwater oceanic turbulence. This enables us to calculate the scintillation index of the annular beam array in underwater environments using our previously developed mathematical model, which is based on the Huygens–Fresnel principle. Thus, the equivalent structure constant for oceanic turbulence is given by [25]

$$C_n^2 = 16\pi^2 k^{-7/6} L^{-11/6}\,\mathrm{Re}\left\{\int_0^L \mathrm{d}\varsigma \int_0^\infty \kappa\,\mathrm{d}\kappa \times \left[E(\varsigma,\kappa,L)E(\varsigma,-\kappa,L) + |E(\varsigma,\kappa,L)|^2\right]\Phi_n(\kappa)\right\}, \quad (3)$$

where $k=2\pi/\lambda$ is the wavenumber, λ is the wavelength, L is the propagation distance, κ is the magnitude of the spatial frequency, the function $E(.)$ and the Nikishov' power spectrum of oceanic turbulence $\Phi_n(\kappa)$ are given respectively,

$$E(\varsigma,\kappa,L) = jk\exp\left[-\frac{0.5j\varsigma(L-\varsigma)\kappa^2}{kL}\right], \quad (4)$$

$$\Phi(\kappa) = 0.388\times 10^{-8}\varepsilon^{-1/3}\kappa^{-11/3}\left[1+2.35(\kappa\eta)^{-2/3}\right] \times \frac{\chi_T}{\omega^2}\left(\omega^2 e^{-A_T\delta} + e^{-A_S\delta} - 2\omega e^{-A_{TS}\delta}\right), \quad (5)$$

where $j=\sqrt{-1}$, ϵ is the rate of dissipation of kinetic energy per unit mass of fluid, η is the Kolmogorov microscale (inner scale), χ_T is the rate of dissipation of mean-squared temperature, ω is the ratio of temperature to salinity contributions to the refractive index spectrum, $A_T = 1.863\times10^{-2}$, $\delta(\kappa,\eta) = 8.284(\kappa\eta)^{4/3} + 12.978(\kappa\eta)^2$, $A_S = 1.9\times10^{-4}$, $A_{TS} = 9.41\times10^{-3}$. It is important to note that the equivalent structure constant provided in (3) has no dependence on height and is only applicable to horizontal underwater links.

2.3. Optical field distribution at the receiver plane

We use the Huygens–Fresnel principle in order to obtain the optical field at the receiver. As stated in [2], the Huygens–Fresnel integral describes the optical field after passing

through a turbulent ocean

$$u_N(\mathbf{p},L) = \frac{k\exp(jkL)}{2\pi jL}\int_{-\infty}^{\infty}\int_{-\infty}^{\infty} u_N(\mathbf{s}) \times \exp\left\{\frac{jk}{2L}\left[(s_x-p_x)^2+(s_y-p_y)^2\right]\right\} \times \exp\left[\psi(\mathbf{s},\mathbf{p})\right] \mathrm{d}s_x\,\mathrm{d}s_y. \quad (6)$$

where $\mathbf{p}=(p_x,p_y)$ is the receiver plane spatial coordinate, $\psi(s,p)$ signifies the random complex phase of a spherical wave while it moves from the source point to the receiver point.

2.4. Optical intensity distribution at the receiver plane

The intensity of an optical beam at the receiver plane can be described as

$$\langle I(\mathbf{p},L)\rangle = \langle u_N(\mathbf{p},L)\,u_N{}^*(\mathbf{p},L)\rangle, \quad (7)$$

By substituting (6) into (7), we find

$$\langle I(\mathbf{p},z=L)\rangle = \left(\frac{k}{2\pi L}\right)^2 \int_{-\infty}^{\infty}\int_{-\infty}^{\infty}\int_{-\infty}^{\infty}\int_{-\infty}^{\infty} \mathbf{ds}_1^2\mathbf{ds}_2^2 \times u_N(\mathbf{s}_1)\,u_N{}^*(\mathbf{s}_2)\exp\left\{\frac{ik}{2L}\left[(\mathbf{p}-\mathbf{s}_1)^2-(\mathbf{p}-\mathbf{s}_2)^2\right]\right\} \times \langle\exp\left[\psi(\mathbf{s}_1,\mathbf{p})\right]\exp\left[\psi^*(\mathbf{s}_2,\mathbf{p})\right]\rangle \quad (8)$$

where the last term representing the ensemble average $<.>$, i.e. long time average is defined as

$$\langle\exp\left[\psi(s_1,\mathbf{p})\right]\exp\left[\psi^*(s_2,\mathbf{p})\right]\rangle = \exp\left[-\frac{1}{2}D(\mathbf{s}_1,\mathbf{s}_2)\right], \quad (9)$$

where $D(s_1,s_2)$ represents the wave structure function with the transverse coordinates of the source. The approximate form of the wave structure function is given by

$$D(\mathbf{s}_1,\mathbf{s}_2) = \frac{2}{\rho_0^2}(\mathbf{s}_1-\mathbf{s}_2)^2. \quad (10)$$

After substituting (9) and (10) into (8), the resulting received intensity expression is expressed as

$$\langle I(\mathbf{p},z=L)\rangle = \left(\frac{k}{2\pi L}\right)^2 \int_{-\infty}^{\infty}\int_{-\infty}^{\infty}\int_{-\infty}^{\infty}\int_{-\infty}^{\infty} \mathbf{ds}_1^2\mathbf{ds}_2^2 \times u_N(\mathbf{s}_1)\,u_N{}^*(\mathbf{s}_2) \times \exp\left\{\frac{\mathrm{i}k}{2L}\left[(\mathbf{p}-\mathbf{s}_1)^2-(\mathbf{p}-\mathbf{s}_2)^2\right]\right\} \times \exp\left[-\frac{1}{\rho_0^2}(\mathbf{s}_1-\mathbf{s}_2)^2\right] \quad (11)$$

where ρ_0 denotes the coherence length of a spherical wave propagating within the turbulence. Here we need to evaluate the integral in order to obtain a closed form expression. To achieve this, we utilize the integral solution of 3.323.210 from Gradshteyn and Ryzhik's book [26]

$$\int_{-\infty}^{\infty}\exp\left(-px^2\pm qx\right)\mathrm{d}x = \exp\left(\frac{q^2}{4p^2}\right)\frac{\sqrt{\pi}}{p}. \quad (12)$$

By substituting (1) into (11) and repeatedly applying (12) to solve (11), we derive the optical intensity of the annular beam array on the axis at the receiver plane as follows

$$\langle I(\mathbf{p}=0,z=L)\rangle = I_1 - I_2 - I_3 + I_4, \quad (13)$$

$$I_1 = A_1^2\exp\left(-\frac{r_0^2}{\alpha_{s1}^2}\right)\left(\frac{k}{2\pi L}\right)^2\frac{\pi^2}{t_1^2t_2^2}\sum_{n=1}^{N}\sum_{m=1}^{M} \times \exp\left(\frac{r_0^2}{4t_2^2\alpha_{s1}^4}\right)\exp\left(\frac{w_{1x}^2+w_{1y}^2}{4t_1^2}\right), \quad (14)$$

$$I_2 = A_1A_2\exp\left(-\frac{r_0^2}{2\alpha_{s1}^2}-\frac{r_0^2}{2\alpha_{s2}^2}\right)\left(\frac{k}{2\pi L}\right)^2\frac{\pi^2}{t_3^2t_4^2}\sum_{n=1}^{N}\sum_{m=1}^{M} \times \exp\left(\frac{r_0^2}{4t_4^2\alpha_{s2}^4}\right)\exp\left(\frac{w_{3x}^2+w_{3y}^2}{4t_3^2}\right), \quad (15)$$

$$I_3 = A_1A_2\exp\left(-\frac{r_0^2}{2\alpha_{s1}^2}-\frac{r_0^2}{2\alpha_{s2}^2}\right)\left(\frac{k}{2\pi L}\right)^2\frac{\pi^2}{t_2^2t_5^2}\sum_{n=1}^{N}\sum_{m=1}^{M} \times \exp\left(\frac{r_0^2}{4t_2^2\alpha_{s1}^4}\right)\exp\left(\frac{w_{5x}^2+w_{5y}^2}{4t_5^2}\right), \quad (16)$$

$$I_4 = A_2^2\exp\left(-\frac{r_0^2}{\alpha_{s2}^2}\right)\left(\frac{k}{2\pi L}\right)^2\frac{\pi^2}{t_7^2t_8^2}\sum_{n=1}^{N}\sum_{m=1}^{M}\exp\left(\frac{r_0^2}{4t_8^2\alpha_{s2}^4}\right) \times \exp\left(\frac{w_{7x}^2+w_{7y}^2}{4t_7^2}\right), \quad (17)$$

where $t_1^2 = \frac{1}{2\alpha_{s1}^2}-\frac{\mathrm{i}k}{2\,\mathrm{L}}+\frac{1}{\rho_0^2}-\frac{1}{t_2^2\,\rho_0^4}$, $t_2^2 = \frac{1}{2\alpha_{s1}^2}+\frac{\mathrm{i}k}{2\,\mathrm{L}}+\frac{1}{\rho_0^2}$, $t_3^2 = \frac{1}{2\alpha_{s1}^2}-\frac{\mathrm{i}k}{2\,\mathrm{L}}+\frac{1}{\rho_0^2}-\frac{1}{t_4^2\,\rho_0^4}$, $t_4^2 = \frac{1}{2\alpha_{s2}^2}+\frac{\mathrm{i}k}{2\,\mathrm{L}}+\frac{1}{\rho_0^2}$, $t_5^2 = \frac{1}{2\alpha_{s2}^2}-\frac{\mathrm{i}k}{2\,\mathrm{L}}+\frac{1}{\rho_0^2}-\frac{1}{t_2^2\,\rho_0^4}$, $t_7^2 = \frac{1}{2\alpha_{s2}^2}-\frac{\mathrm{i}k}{2\,\mathrm{L}}+\frac{1}{\rho_0^2}-\frac{1}{t_8^2\,\rho_0^4}$, $t_8^2 = \frac{1}{2\alpha_{s2}^2}+\frac{\mathrm{i}k}{2\,\mathrm{L}}+\frac{1}{\rho_0^2}$, $w_{1x} = \frac{r_0\,\cos\theta_n}{\alpha_{s1}^2}+\frac{r_0\,\cos\theta_m}{t_2^2\,\alpha_{s1}^2\,\rho_0^2}$, $w_{3x} = \frac{r_0\,\cos\theta_n}{\alpha_{s1}^2}+\frac{r_0\,\cos\theta_m}{t_4^2\,\alpha_{s2}^2\,\rho_0^2}$, $w_{5x} = \frac{r_0\,\cos\theta_n}{\alpha_{s2}^2}+\frac{r_0\,\cos\theta_m}{t_2^2\,\alpha_{s1}^2\,\rho_0^2}$, $w_{7x} = \frac{r_0\,\cos\theta_n}{\alpha_{s2}^2}+\frac{r_0\,\cos\theta_m}{t_8^2\,\alpha_{s2}^2\,\rho_0^2}$. Note that w_{1y}, w_{3y}, w_{5y}, and w_{7y} are obtained by replacing the cosine function in w_{1x}, w_{3x}, w_{5x}, and w_{7x} with the sine function, respectively.

2.5. Scintillation index

Scintillation refers to the fluctuations in the received intensity. These fluctuations are measured by calculating the scintillation index, which is expressed as follows

$$m^2 = \frac{\langle I^2\rangle}{\langle I\rangle^2}-1, \quad (18)$$

To calculate the scintillation index of the annular beam array, we require the received intensity <I>, which is already provided in (13), along with $<I^2>$, defined as follows [27]

$$\begin{aligned}\left\langle I^2(L)\right\rangle = \frac{1}{(\lambda L)^4}&\int_{-\infty}^{\infty}\int_{-\infty}^{\infty}\mathrm{d}^2 s_1\int_{-\infty}^{\infty}\int_{-\infty}^{\infty}\mathrm{d}^2 s_2\\ &\times\int_{-\infty}^{\infty}\int_{-\infty}^{\infty}\mathrm{d}^2 s_3\int_{-\infty}^{\infty}\int_{-\infty}^{\infty}\mathrm{d}^2 s_4\\ &\times u_{Ns}(s_1)\,u_{Ns}^{*}(s_2)\,u_{Ns}(s_3)\,u_{Ns}^{*}(s_4)\\ &\times\exp\left[\frac{jk}{2L}\left(|s_1|^2-|s_2|^2+|s_3|^2-|s_4|^2\right)\right]\\ &\times F_4(\mathbf{s}_1,\mathbf{s}_2,\mathbf{s}_3,\mathbf{s}_4),\end{aligned}\tag{19}$$

where $F_4(s_1,s_2,s_3,s_4)$ is the fourth-order spherical-wave coherence function which is given by [27]

$$\begin{aligned}&F_4(s_1,s_2,s_3,s_4)\\ &=\exp\left[2B_\chi(s_1-s_3)+2B_\chi(s_2-s_4)\right.\\ &\quad-\frac{1}{2}D_\psi(s_1-s_2)-\frac{1}{2}D_\psi(s_1-s_4)-\frac{1}{2}D_\psi(s_2-s_3)\\ &\quad-\frac{1}{2}D_\psi(s_3-s_4)+\frac{1}{2}D_\psi(s_1-s_3)+\frac{1}{2}D_\psi(s_2-s_4)\\ &\quad\left.+jD_{\chi S}(s_2-s_4)-jD_{\chi S}(s_1-s_3)\right]\end{aligned}\tag{20}$$

Here, $B_\chi(\mathbf{s}_r-\mathbf{s}_q)=\sigma_{\chi_s}^2-\frac{1}{2}\left(\frac{1}{\rho_0^2}-\frac{1}{\rho_\chi^2}\right)(\mathbf{s}_r-\mathbf{s}_q)^2$ is the log amplitude correlation function, $D_\psi(s_r-s_q)=2\rho_0^{-2}(s_r-s_q)^2$ is the wave structure function, $D_{\chi S}(s_r-s_q)=\rho_{\chi S}^{-2}(s_r-s_q)^2$ is the log-amplitude and phase structure function, $r=1,2$ and $q=3,4$ and $\sigma_{\chi_s}^2=0.124k^{7/6}C_n^2L^{11/6}$ is the spherical wave log-amplitude variance and $\rho_\chi=(0.425C_n^2k^{13/6}L^{5/6})^{-1/2}$, $\rho_{\chi S}=(0.114C_n^2k^{13/6}L^{5/6})^{-1/2}$ is the coherence length of log-amplitude and phase. It should be noted that $\sigma_{\chi_s}^2$, ρ_χ, and $\rho_{\chi S}$ are well-established results from atmospheric turbulence theory, derived using the Kolmogorov spectrum and the Rytov approximation. By employing the equivalent structure constant in calculating these parameters, we are able to directly apply the existing formulations. Without the use of the equivalent structure constant, these parameters would instead need to be derived from the Nikishov's underwater turbulence spectrum or other spectral models. It should also be noted that the wave structure function is valid in the range of $l_0\ll|\mathbf{s}_d|\ll\sqrt{\lambda L}$, where l_0 is the inner scale of turbulence, $|\mathbf{s}_d|$ is the difference of the source transverse coordinates, $\sqrt{\lambda L}$ is the Fresnel zone. By repeatedly applying (12), we have derived a solution for (19), which is

$$\begin{aligned}\left\langle I^2(p,L)\right\rangle = \exp\left\{4\sigma_{\chi_s}^2\right\}&\frac{1}{(\lambda L)^4}\sum_{n=1}^{N}\\ &\times\sum_{m=1}^{M}\sum_{o=1}^{O}\sum_{u=1}^{U}\sum_{n1=1}^{2}\sum_{m1=1}^{2}\sum_{o1=1}^{2}\sum_{u1=1}^{2}A_{n1}A_{m1}A_{o1}A_{u1}\\ &\times\exp\left[-\frac{r_0^2}{2}\left(\frac{1}{\alpha_{sn1}^2}+\frac{1}{\alpha_{sm1}^2}+\frac{1}{\alpha_{so1}^2}+\frac{1}{\alpha_{su1}^2}\right)\right]I_x^2I_y^2\end{aligned}\tag{21}$$

where

$$\begin{aligned}I_x^2=&\frac{\pi^2}{\beta_1\beta_2\beta_3\beta_4}\exp\left(\frac{q_{1x}^2}{4\beta_1^2}+\frac{Y_x^2}{4\beta_2^2}\right)\exp\left(\frac{r_0^2\cos^2\theta_u}{4\beta_4^2\alpha_{su1}^4}\right)\\ &\times\exp\left[\frac{r_0^2}{4\beta_3^2}\left(\frac{\cos^2\theta_o}{\alpha_{so1}^4}+\frac{\cos^2\theta_u}{\beta_4^4\alpha_{su1}^4\rho_0^4}+2\frac{\cos\theta_o\cos\theta_u}{\beta_4^2\alpha_{su1}^2\alpha_{so1}^2\rho_0^2}\right)\right],\end{aligned}\tag{22}$$

$$\begin{aligned}I_y^2=&\frac{\pi^2}{\beta_1\beta_2\beta_3\beta_4}\exp\left(\frac{q_{1y}^2}{4\beta_1^2}+\frac{Y_y^2}{4\beta_2^2}\right)\exp\left(\frac{r_0^2\sin^2\theta_u}{4\beta_4^2\alpha_{su1}^4}\right)\exp\\ &\times\left[\frac{r_0^2}{4\beta_3^2}\left(\frac{\sin^2\theta_o}{\alpha_{so1}^4}+\frac{\sin^2\theta_u}{\beta_4^4\alpha_{su1}^4\rho_0^4}+2\frac{\sin\theta_o\sin\theta_u}{\beta_4^2\alpha_{su1}^2\alpha_{so1}^2\rho_0^2}\right)\right].\end{aligned}\tag{23}$$

Here $\beta_4^2=\frac{1}{2\alpha_{su1}^2}+\frac{jk}{2L}+\frac{2}{\rho_0^2}-\frac{1}{\rho_\chi^2}-\frac{j}{\rho_{\chi S}^2}$, $\beta_3^2=\frac{1}{2\alpha_{so1}^2}-\frac{1}{\beta_4^2\rho_0^4}-\frac{jk}{2L}+\frac{2}{\rho_0^2}-\frac{1}{\rho_\chi^2}+\frac{j}{\rho_{\chi S}^2}$, $\beta_2^2=\frac{2}{\rho_0^2}-\frac{1}{\rho_\chi^2}-\frac{j}{\rho_{\chi S}^2}+\frac{jk}{2L}+\frac{1}{2\alpha_{sm1}^2}-\frac{1}{\beta_4^2}R^2-\frac{1}{\beta_3^2\rho_0^4}\left(1-\frac{R}{\beta_4^2}\right)^2$, $\beta_1^2=\frac{2}{\rho_0^2}-\frac{1}{\rho_\chi^2}+\frac{j}{\rho_{\chi S}^2}-\frac{jk}{2L}+\frac{1}{2\alpha_{sn1}^2}-\frac{1}{\beta_4^2\rho_0^4}-\frac{T^2}{\beta_3^2}-\frac{X^2}{4\beta_2^2}$, $T=-\frac{1}{\rho_\chi^2}+\frac{j}{\rho_{\chi S}^2}+\frac{1}{\beta_4^2\rho_0^4}$, $X=\frac{2}{\rho_0^2}-\frac{2R}{\beta_4^2\rho_0^2}+\frac{2T}{\beta_3^2\rho_0^2}\left(1-\frac{R}{\beta_4^2}\right)$, $R=\frac{1}{\rho_\chi^2}+\frac{j}{\rho_{\chi S}^2}$, $q_{1x}=\frac{r_0\cos\theta_n}{\alpha_{sn1}^2}+\frac{r_0\cos\theta_u}{\beta_4^2\alpha_{su1}^2\rho_0^2}+\frac{Tr_0\cos\theta_o}{\beta_3^2\alpha_{so1}^2}+\frac{Tr_0\cos\theta_u}{\beta_3^2\beta_4^2\alpha_{su1}^2\rho_0^2}+\frac{XY_x}{2\beta_2^2}$, $Y_x=\frac{r_0\cos\theta_m}{\alpha_{sm1}^2}-\frac{r_0\cos\theta_uR}{\beta_4^2\alpha_{su1}^2}+\frac{r_0\cos\theta_o}{\beta_3^2\alpha_{so1}^2\rho_0^2}\left(1-\frac{R}{\beta_4^2}\right)+\left(1-\frac{R}{\beta_4^2}\right)\frac{r_0\cos\theta_u}{\rho_0^4\beta_3^2\beta_4^2\alpha_{su1}^2}$. Note that $q_{1}y$ and Yy are obtained by replacing the cosine function in $q_{1}x$ and Yx with the sine function, respectively.

3. Numerical results

In this section, we have attempted to show how multiple annular beams affect the reduction of scintillation. In the simulations we presented, the laser sources are set to a wavelength of $\lambda=0.532\,\mu$m, unless stated otherwise. We present the scintillation index of the single annular beam $(N=1)$ in all the figures as a benchmark. For the single beam case, $N=1$, we set the ring radius to zero $(r_0=0)$ to emphasize the effects of transmit diversity over a perfectly aligned single-input single-output (SISO) UOWC system. It is important to note that since our scintillation formulations are applicable in weak oceanic turbulence, we aimed to meet the weak turbulence condition $\sigma_R^2=1.23C_n^2k^{7/6}L^{11/6}<1$ in our simulations, using the equivalent structure constant derived in (3). We would also like to point out that the transmitter source size and ring radius were selected to be physically small in order to maintain the validity range of the wave structure function. We can validate the correctness of our derived scintillation index formula by setting the field amplitude of the secondary beam to zero, $A_2=0$, which corresponds to our previously reported results in the literature [17].

In figure 2, we plot the scintillation of the annular beam array versus the ratio of temperature to salinity contributions to the refractive index spectrum ω. The scintillation index of the annular beam for SISO case $N=1$, $r_0=0$ is also plotted as

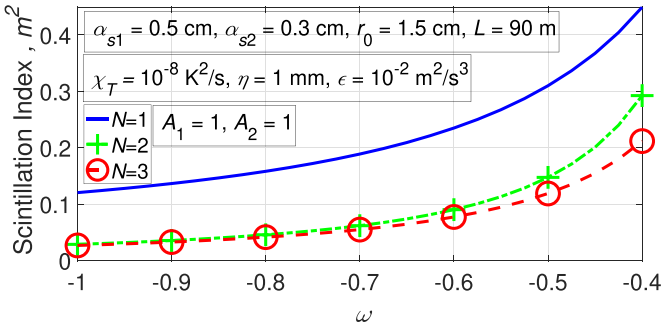

Figure 2. Scintillation index m^2 versus the ratio of temperature to salinity contributions to the refractive index spectrum ω for various N values.

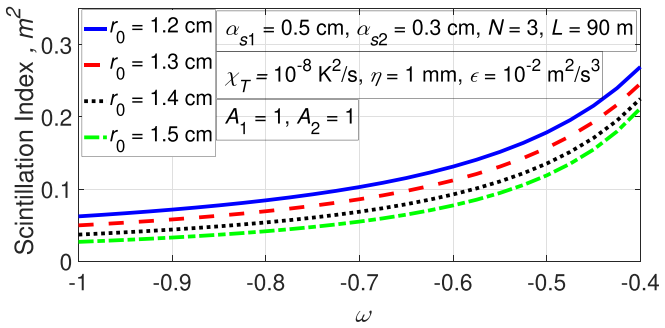

Figure 3. Scintillation index m^2 versus ω for various ring radius r_0 values.

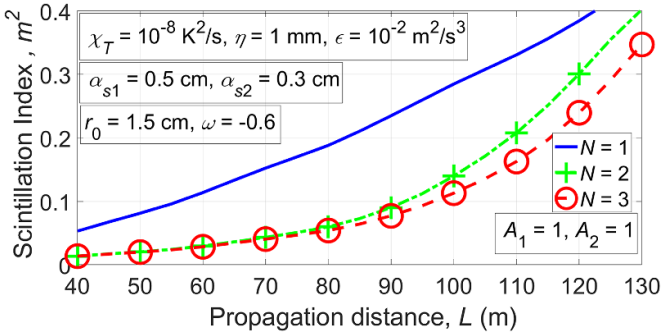

Figure 4. Scintillation index m^2 versus propagation distance L for various N values.

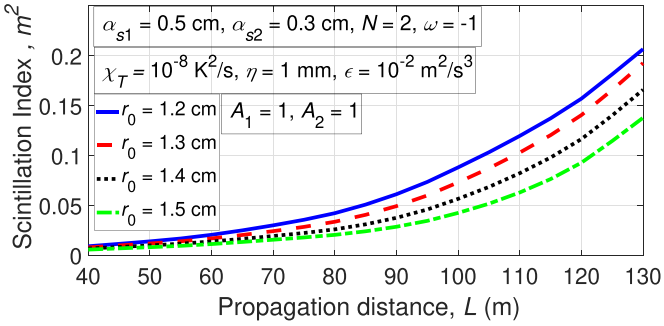

Figure 5. Scintillation index m^2 versus propagation distance L for various radius r_0 values.

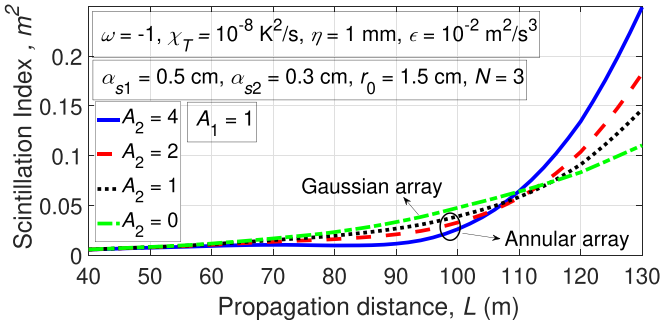

Figure 6. Scintillation index m^2 versus propagation distance L for various A_2 values.

a benchmark. It is found that as the parameter ω increases, an increase in the scintillation index is observed. This is an expected result, as higher salinity levels lead to increased turbulence, which in turn causes an increase in scintillation. It is clear that the reduction in scintillation due to spatial diversity is achieved by increasing the number of annular laser beams. This reduction becomes evident at higher levels of ω. In figure 3, the system parameters are kept the same as in figure 2, except that the number of beams is fixed at $N = 3$, while the ring radius r_0 is varied. We have observed that an increase in the ring radius r_0 leads to a decrease in the scintillation index. The underlying physical explanation for this trend is that as the ring radius r_0 grows, the distance between the beams increases, causing each beam to experience statistically different channels, which in turn reduces scintillation.

In figure 4, the scintillation index is plotted against the propagation distance for various values of N. As seen in figure 4, the scintillation index increases with the increase in the propagation distance L. It is clear that increasing the number of beams leads to a reduction in scintillation. In figure 5, with the number of beams fixed at $N = 2$ and the ring radius of the array r_0 varied, we plot the scintillation index against the propagation distance. We observe similar results as in figure 3, where an increase in the ring radius leads to a decrease in the scintillation index. We would like to highlight how the spacing between the annular lasers affects the scintillation index shown in figure 5. When $N = 2$ the two annular beams are positioned 180 degrees apart on the ring, resulting in the maximum separation, with twice the ring radius directly representing this distance. For $N = 3$ in our simulations, which are not included in the paper, the scintillation index continues to decrease as the ring radius increases; however, determining the exact distance between the beams in this case requires additional effort.

In figure 6, we have compared the scintillation index behavior of annular beam array and the Gaussian beam array. Here we note that when $A_2 = 0$, our scintillation formulation in (18) reduces to laser array beam scintillation given in (8) of [17]. This allows us to make a comparison. In figure 6 we find that the annular beam array performs better than the Gaussian beam arrays in reducing scintillation up to a propagation distance of 110 meters; beyond this point, the Gaussian beam array begins to outperform the annular beam arrays.

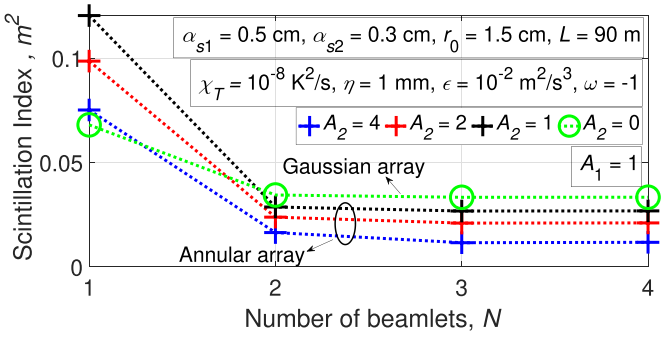

Figure 7. Scintillation index m^2 versus number of beamlets N for various A_2 values.

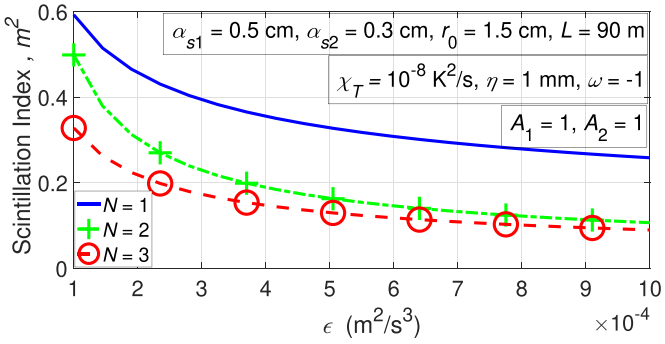

Figure 8. Scintillation index m^2 versus the rate of dissipation of kinetic energy per unit mass of fluid ϵ for various N values.

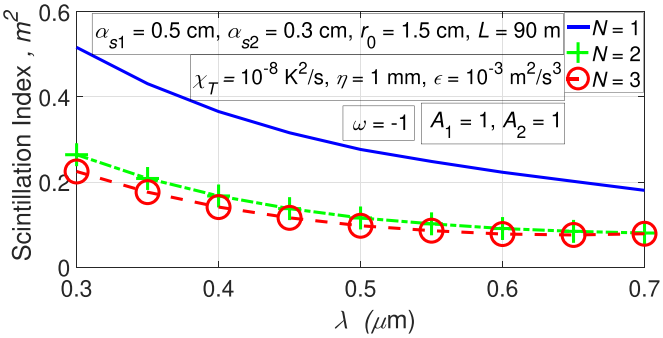

Figure 9. Scintillation index m^2 versus the wavelength λ for various N values.

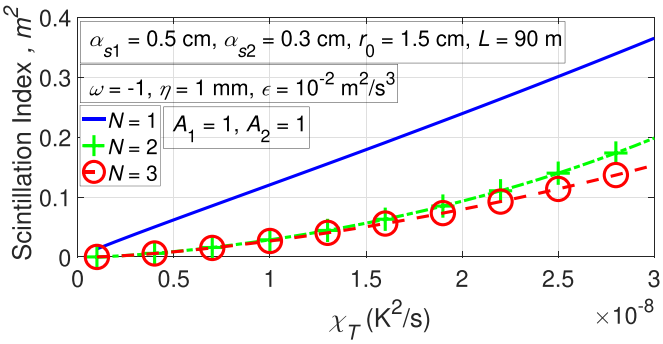

Figure 10. Scintillation index m^2 versus the rate of dissipation of the mean squared temperature χ_T for various N values.

From figure 6, it is observed that increasing the field amplitude of the secondary beam in the annular array leads to a reduction in scintillation for propagation distances below $L = 105$ m, while for distances beyond $L = 105$ m, the scintillation index increases significantly. Note that, in this study, the annular beam array inherently represents both transmit spatial diversity and beam shaping, whereas the Gaussian beam array represents only transmit spatial diversity. As shown in figure 6, combining these two approaches yields lower scintillation than using spatial diversity method alone, up to $L = 105$ m.

In figure 7, the scintillation index versus number of beams in the array is plotted for various A_2 values. It is observed that as the number of beams in the array increases, the scintillation index decreases. The scintillation index also decreases as the field amplitude of the secondary source size A_2 increases. It is interesting to note that the annular beam array is better than the Gaussian beam array for the reduction of scintillation. However, when considering a single beam $N = 1$, $r_0 = 0$ the scintillation of the single Gaussian beam is better than that of the single annular beam for the specified system parameters presented in figure 7. The physical reason for this behavior is that a single annular beam diverges more than a Gaussian beam. Consequently, both the average intensity and the average of intensity square decrease; however, since the scintillation index is determined by their ratio, it tends to increase due to these variations.

In figure 8, we aimed to demonstrate the effect of the oceanic turbulence parameter, specifically the rate of kinetic energy dissipation per unit mass of fluid, ϵ, on the scintillation index for different numbers of beams. figure 8 shows that an increase in ϵ leads to a decrease in scintillation. Additionally, further reductions in scintillation are observed with an increase in the number of beams N in the array.

In figure 9, the scintillation index is shown as a function of the source wavelength λ for various N values. It is apparent in figure 9 that transmit diversity contributes to a decrease in scintillation. Additionally, we observe that the scintillation index decreases as the wavelength increases. Notably, visible wavelengths are employed in underwater optical communications, with the blue-green region of the spectrum preferred because it experiences minimal absorption and scattering underwater. For this reason, we have chosen $\lambda = 0.532$ for our simulation presented in this section.

Finally, in figure 10, we have plotted the scintillation index against the underwater turbulence parameter, specifically the rate of dissipation of the mean squared temperature χ_T, for different values of N. It is observed that as χ_T increases, the scintillation index also increases. At a fixed χ_T value, the lowest scintillation index is seen when the number of beams in the array is chosen as $N = 3$.

4. Conclusion

In this paper, we have developed formulas to calculate the scintillation index of the annular beam array in underwater turbulence. To do this, we expressed the effective structure constant in terms of underwater turbulence parameters, referring to it

as the equivalent structure constant. Utilizing the Huygens–Fresnel principle, we first derived the average intensity along the axis at the receiver and then calculated the average of the square of the intensity along the same axis. Finally, we used these two quantities to evaluate the scintillation index, which is presented in the numerical results section. It should be noted that our results are limited to the weak fluctuations. For this reason, we aimed to meet the weak turbulence condition $\sigma_R^2 = 1.23C_n^2k^{7/6}L^{11/6} < 1$ in our simulations.

In the study, we observed that as the number of annular beams, ring radius, inner beam amplitude, wavelength, and the rate of kinetic energy dissipation per unit mass of fluid increase, the scintillation index decreases. Conversely, the scintillation index increases when the ratio of temperature to salinity contributions to the refractive index spectrum, propagation distance, and rate of dissipation of mean squared temperature rise. Additionally, the annular beam array outperforms the Gaussian beam array in terms of scintillation index up to 110 m.

The findings in this paper will assist system designers in understanding how beam shaping and spatial diversity impact the scintillation performance of an UOWC system operating under weak oceanic turbulence.

Data availability statement

The data that support the findings of this study are available upon reasonable request from the authors.

Author contributions

Ekin Erdoğdu
Conceptualization (equal), Formal analysis (equal), Investigation (equal), Methodology (equal), Software (equal), Visualization (equal), Writing – original draft (equal)

Muhsin Caner Gökçe 0000-0003-4465-1983
Conceptualization (equal), Formal analysis (equal), Investigation (equal), Methodology (equal), Software (equal), Supervision (equal), Visualization (equal), Writing – original draft (equal), Writing – review & editing (equal)

Yahya Baykal 0000-0002-4897-0474
Conceptualization (equal), Formal analysis (equal), Methodology (equal), Supervision (equal), Writing – original draft (equal), Writing – review & editing (equal)

References

[1] Ali M F, Jayakody D N K and Li Y 2022 Recent trends in underwater visible light communication (UVLC) systems *IEEE Access* **10** 22169–225
[2] Baykal Y, Ata Y and Gökçe M C 2022 Underwater turbulence, its effects on optical wireless communication and imaging: a review *Opt. Laser Technol.* **156** 108624
[3] Kaushal H and Kaddoum G 2016 Underwater optical wireless communication *IEEE Access* **4** 1518–47
[4] Morel A and Prieur L 1977 Analysis of variations in ocean color 1 *Limnol. Oceanogr.* **22** 709–22
[5] Haltrin V I 1999 Chlorophyll-based model of seawater optical properties *Appl. Opt.* **38** 6826–32
[6] Khalighi M A and Uysal M 2014 Survey on free space optical communication: a communication theory perspective *IEEE Commun. Surv. Tutor.* **16** 2231–58
[7] Korotkova O 2019 Light propagation in a turbulent ocean *Progress in Optics* vol 64 (Elsevier) pp 1–43
[8] Gökçe M C and Baykal Y 2018 Aperture averaging and BER for Gaussian beam in underwater oceanic turbulence *Opt. Commun.* **410** 830–5
[9] Ata Y, Gökçe M C and Baykal Y 2024 Intelligent reflecting surface aided vehicular optical wireless communication systems using higher-order mode in underwater channel *IEEE Trans. Veh. Technol.* **73** 11196–208
[10] Cai Y 2011 Generation of various partially coherent beams and their propagation properties in turbulent atmosphere: a review *Atmos. Ocean. Propag. Electromagn. Waves V* **7924** 7–22
[11] Avramov-Zamurovic S and Nelson C 2018 Experimental study: underwater propagation of polarized flat top partially coherent laser beams with a varying degree of spatial coherence *Opt. Commun.* **424** 54–62
[12] Salcedo-Serrano P, Boluda-Ruiz R, Garrido-Balsells J M, García-Zambrana A and Hranilovic S 2023 Underwater optical wireless channel capacity under oceanic turbulence using spatial diversity techniques *ICC 2023 - IEEE Int. Conf. on Communications* pp 1162–8
[13] Huang A, Tao L, Wang C and Zhang L 2018 Error performance of underwater wireless optical communications with spatial diversity under turbulence channels *Appl. Opt.* **57** 7600–8
[14] Yue P, Hu J, Yi X, Luan X and Xu D 2019 Wave optics simulation investigation of multiple-input and aperture-averaging for optical wave propagation in turbulent ocean *Opt. Commun.* **452** 327–33
[15] Cui Z, Yue P, Yi X and Li J 2021 Effect of convergent beam array on reducing scintillation in underwater wireless optical communications with pointing errors *Opt. Express* **29** 9846–60
[16] Cui Z, Yue P, Yi X and Li J 2022 Improving the performance of underwater wireless optical communications by pointing adjustable beam arrays *IEEE Trans. Veh. Technol.* **72** 483–97
[17] Gökçe M C and Baykal Y 2016 Scintillation analysis of multiple-input single-output underwater optical links *Appl. Opt.* **55** 6130–6
[18] Gökçe M C, Baykal Y and Uysal M 2016 Performance analysis of multiple-input multiple-output free-space optical systems with partially coherent Gaussian beams and finite-sized detectors *Opt. Eng., Bellingham* **55** 111607
[19] Gökçe M C, Baykal Y and Uysal M 2016 Aperture averaging in multiple-input single-output free-space optical systems using partially coherent radial array beams *J. Opt. Soc. Am. A* **33** 1041–8
[20] Boucouvalas A C, Peppas K P, Yiannopoulos K and Ghassemlooy Z 2016 Underwater optical wireless communications with optical amplification and spatial diversity *IEEE Photonics Technol. Lett.* **28** 2613–6
[21] Ata Y, Baykal Y and Gökçe M C 2024 Analysis of optical wireless MIMO communication in underwater medium *IEEE Internet Things J.* **11** 20660–72
[22] Jamali M V, Salehi J A and Akhoundi F 2016 Performance studies of underwater wireless optical communication systems with spatial diversity: MIMO scheme *IEEE Trans. Commun.* **65** 1176–92
[23] Jamali M V, Nabavi P and Salehi J A 2018 MIMO underwater visible light communications: comprehensive channel study, performance analysis and multiple-symbol detection *IEEE Trans. Veh. Technol.* **67** 8223–37

[24] Jiang H, Qiu H, He N, Popoola W, Ahmad Z and Rajbhandari S 2020 Performance of spatial diversity DCO-OFDM in a weak turbulence underwater visible light communication channel *J. Lightwave Technol.* **38** 2271–7
[25] Baykal Y 2016 Expressing oceanic turbulence parameters by atmospheric turbulence structure constant *Appl. Opt.* **55** 1228–31
[26] Gradshteyn I S and Ryzhik I M 2014 *table of Integrals, Series and Products* (Academic) (https://doi.org/10.1016/C2010-0-64839-5)
[27] Wang S, Baykal Y and Plonus M 1983 Receiver-aperture averaging effects for the intensity fluctuation of a beam wave in the turbulent atmosphere *J. Opt. Soc. Am.* **73** 831–7